

Laboratory apparatus for in-situ corrosion fatigue testing and characterisation of fatigue cracks using X-ray micro-computed tomography

Farhad, F., Smyth-Boyle, D., Zhang, X., Wallis, I. & Panggabean, D.

Author post-print (accepted) deposited by Coventry University's Repository

Original citation & hyperlink:

Farhad, F, Smyth-Boyle, D, Zhang, X, Wallis, I & Panggabean, D 2018, 'Laboratory apparatus for in-situ corrosion fatigue testing and characterisation of fatigue cracks using X-ray micro-computed tomography', *Fatigue and Fracture of Engineering Materials and Structures*, vol. 41, no. 12, pp. 2629-2637.

<https://dx.doi.org/10.1111/ffe.12873>

DOI [10.1111/ffe.12873](https://dx.doi.org/10.1111/ffe.12873)

ISSN 8756-758X

ESSN 1460-2695

Publisher: Wiley

This is the peer reviewed version of the following article: Farhad, F, Smyth-Boyle, D, Zhang, X, Wallis, I & Panggabean, D 2018, 'Laboratory apparatus for in-situ corrosion fatigue testing and characterisation of fatigue cracks using X-ray micro-computed tomography' *Fatigue and Fracture of Engineering Materials and Structures*, vol 41:12, pp. 2629-2637, which has been published in final form at <https://dx.doi.org/10.1111/ffe.12873>

This article may be used for non-commercial purposes in accordance with Wiley Terms and Conditions for Self-Archiving.

Copyright © and Moral Rights are retained by the author(s) and/ or other copyright owners. A copy can be downloaded for personal non-commercial research or study, without prior permission or charge. This item cannot be reproduced or quoted extensively from without first obtaining permission in writing from the copyright holder(s). The content must not be changed in any way or sold commercially in any format or medium without the formal permission of the copyright holders.

This document is the author's post-print version, incorporating any revisions agreed during the peer-review process. Some differences between the published version and this version may remain and you are advised to consult the published version if you wish to cite from it.

1
2
3 **Laboratory apparatus for *in-situ* corrosion fatigue testing and characterisation of**
4 **fatigue cracks using X-ray micro-computed tomography**
5
6
7
8

9 F. Farhad^{1,2,*}, D. Smyth-Boyle³, X. Zhang², I. Wallis³, D. Panggabean³
10

11 1- National Structural Integrity Research Centre (NSIRC), Cambridge, UK

12 2- Faculty of Engineering, Environment and Computing, Coventry University, Coventry,
13 UK
14

15 3- The Welding Institute Ltd. (TWI), Cambridge, UK
16
17

18 * Corresponding Author: Address: NSIRC, Granta Park, Cambridge, CB21 6AL
19
20

21
22
23 **ABSTRACT**
24

25
26 This paper presents the design, construction and assembly of laboratory apparatus to
27 undertake *in-situ* corrosion fatigue tests in a sour corrosive environment under uniaxial
28 fatigue loading. The bespoke test cell allows non-destructive X-ray micro-computed
29 tomography of the specimen *in-situ* during fatigue testing and thus enables monitoring of
30 material degradation as it progresses and in particular the pit-to-crack transition. This
31 approach provides more direct information on crack initiation than complementary *ex-situ*
32 techniques such as Scanning Electron Microscopy (SEM) of post-test metallographic
33 specimens. Moreover, the apparatus was designed to allow a fatigue cycle to be interrupted
34 and maintain the sample under static tensile load, during X-ray tomography scans. This
35 process reduced the risk of premature crack closure during interrupted tests. Results
36 presented herein demonstrate the performance and reliability of our approach and will
37 hopefully stimulate other groups to employ similar 'lab-scale' initiatives.
38
39
40
41
42
43
44
45
46
47
48
49

50 **Keywords:** Fatigue crack initiation, Pitting corrosion, Corrosion fatigue experiment, Crack
51 monitoring, Environmental technique
52
53
54
55
56
57

1. Introduction

Pipelines used to transport oil and gas are commonly manufactured from API-5L X65 steel. Pipes are typically subjected to cyclic loading and the internal surfaces are often exposed to sour corrosive environments. The latter condition can induce a form of localized corrosion damage termed pitting. Corrosion pits are often sites for initiation of fatigue cracks. The transition from corrosion pit to fatigue crack, the so-called pit-to-crack transition, is a significant part of the total fatigue life and yet the underlying mechanism is not well understood. In order to better understand the pit-to-crack transition and provide further clarity regarding the overall process of corrosion fatigue, it is important to conduct testing under conditions representative of the field environment and service loading.

The material of interest in this study is API-5L X65 steel, which is commonly used for oil and gas pipelines¹. Although this steel grade is attractive in terms of mechanical properties, cost and availability, it is susceptible to pitting corrosion in sour environments that can lead to failure of pipelines^{2,3}. Pitting is an insidious form of localized corrosion, as in addition to accelerated material loss over a small area, pitting can introduce stress raisers and thus increase the risk of crack initiation and ultimately failure of engineering assets. The transition of corrosion pitting to fatigue cracking, the pit-to-crack transition, is a significant part of the total fatigue life⁴ and yet the mechanism involved is not well understood. Investigations on corrosion pit-to-crack transitions have received growing attention in recent years due to its vital role in corrosion fatigue life⁵. Understanding this transition is critical in order to improve corrosion fatigue prediction models.

Previous studies have investigated the pit-to-crack transition stage using *ex-situ* surface methods such as light microscopy or Scanning Electron Microscope (SEM) to probe the exterior of the material intermittently during and after fatigue testing⁶⁻⁹. However, this method is quite limited and observation and monitoring of cracks initiated within the pit wall or base of the pit are not possible using this approach. In recent years there has been an increasing interest in characterising materials using laboratory-based or synchrotron-based X-ray Computed Tomography (CT) and the applicability of this technique in materials science is well established¹⁰. One obvious advantage of this approach is that it is a non-destructive method. Synchrotron-based X-ray CT has been used to study the mechanical performance of materials under static loading^{10,11}, cyclic loading^{12,13}, corrosion-fatigue condition and even to evaluate the localized corrosion rate of inclusions in alloys¹⁴. Horner and co-workers¹⁵

utilized *ex-situ* laboratory-based X-ray tomography to characterize the cracks initiated from corrosion pits under tensile loads. However, the availability of the synchrotron beamlines is limited and has been an issue ¹⁶.

Oil and gas production pipelines often operate under sour corrosive environments in combination with cyclic loading. It is well known that an aggressive environment can reduce the fatigue life of materials ¹⁷. Consequently, it is important to replicate in-service conditions during testing to obtain reliable data regarding corrosion fatigue behaviour and in particular pit-to-crack transitions in X65 steel pipelines. Wang and Akid ¹⁸, Akid and Dmytrakh ¹⁹, Arriscorreta ²⁰, Baragetti ²¹, Li and Akid²² have used chambers to expose the sample to saline solutions (NaCl) during fatigue tests. The corrosion mini-cell used by Akid and Dmytrakh exposes the sample to 0.3cm³ of artificial seawater and is open to the atmosphere. Their tests were carried out under uniaxial fatigue loading. Li and Akid utilised a rubber chamber for undertaking 4-point rotating bending corrosion fatigue tests. The low volume environmental chamber designed by Arriscorreta enabled continuous flow of test solution to ensure that the test environment was replenished during corrosion fatigue tests. Baragetti exposed the sample notch area to NaCl solution by bolting two pieces of Plexiglass shells around the sample. The described environmental chambers were useful for corrosion fatigue tests in NaCl solutions, however these chambers are not practical for testing in an environment including the toxic gas of H₂S because the required chamber needs to be sealed securely. Also, they were not applicable for the purpose of *in-situ* X-ray tomography. Due to the challenges in experimental testing (including the Health and Safety considerations, as H₂S is toxic) the effect of sour environments on the mechanism of fatigue crack initiation has not been addressed by researchers. Therefore, a primary aim of this study was to carry out uniaxial fatigue tests in the sour corrosive environment.

To the best of our knowledge, no studies have been conducted to (a) carry out small-scale corrosion fatigue tests using specimens presenting a single defined pit exposed to an aqueous sour environment and (b) utilize laboratory-based X-ray CT to monitor the nucleation of fatigue cracks induced from corrosion pits during *in-situ* corrosion fatigue tests. This paper details the development of environmental apparatus to facilitate the aforementioned tests and thereby visualise the evolution of a fatigue crack from a corrosion pit in X65 steel using X-ray CT. To acquire tomography data during experiments, a novel '*in-situ* interrupted test' protocol was developed whereby the test specimen under load was imaged at defined

1
2
3 intervals. In the present paper, design features and some representative results from recent
4 experiments are presented and the advantages and limitations of our approach discussed.
5

6 7 **2. Environmental cell and ancillaries**

8
9 The test cell comprises five main elements, viz. the vessel body, vessel lids, locking rings,
10 followers and grippers. A schematic of the cell is given in Figure 1.
11

12
13 The vessel body was machined from a transparent cast acrylic (poly(methyl methacrylate))
14 tube (Perspex). Similar designs for the basic vessel body have been reported by Williams *et*
15 *al.*¹², Singh *et al.*²³ and Chapman *et al.*²⁴. Perspex was selected as the most suitable material
16 of choice on the grounds of chemical, mechanical and optical properties. Crucially, Perspex is
17 resistant to chemical degradation in saline solutions containing dissolved H₂S and has
18 excellent X-ray transmission properties. This material has been used as a material of
19 construction for vessels used in X-ray scanners^{11,24,25}. The optical transparency of Perspex
20 provides the same practical advantages as glass, including clear observation of the sample in
21 the test cell during set up of the location parameters and region of interest in the X-ray
22 scanner, in addition to enabling visual inspection of the test solution in the vessel (i.e. level
23 checks during solution transfer, indication of solution loss, changes in colour or clarity, etc).
24 The anticipated mechanical loads placed on the vessel required minimum wall thickness
25 values of around 5mm. However, additional considerations led to the decision to use a value
26 of 10mm. These factors included the need to provide further assurance that the test cell would
27 not distort during specimen loading (i.e. under the compression load applied via the vertical
28 bolts placed in the grippers as the latter maintain the tensile load on the sample). Increased
29 wall thickness also reduced concerns regarding the modest creep strength of Perspex. Finally,
30 the increase in dimension was necessary in order to provide an O-ring groove around the
31 circumference.
32

33
34 The provision of robust sealing for the test cell was a vital consideration, due to the toxic
35 nature of the H₂S contained therein and the need to exclude oxygen from the test
36 environment. The configuration employed in this work ensured that the contents of the cell
37 were fully isolated from the external environment throughout testing using axially loaded
38 small-scale tensile specimens. Sealing was achieved using two O-ring pairs. One pair of O-
39 rings (14x1.5 VI75 type) are located around the sample top and bottom, between the vessel
40 lid and the elliptical follower and sit inside the vessel lid groove. The second pair (75x2.5
41 VI75 type) sit in grooves located in the top and bottom of the vessel body and placed between
42
43
44

1
2
3 the vessel body and the vessel lid. Prior to placement, O-rings were lubricated with a clear
4 silicon grease to reduce interfacial friction. By placing all the followers, tightening screws
5 and locking rings, the O-rings were held in place and sealing was ensured.
6
7

8 The top and bottom vessel lids were machined from PEEK (polyether ether ketone), a
9 thermoplastic with excellent mechanical properties and chemical resistance to corrosive sour
10 environments. Four ports were machined to allow for entry and exit of both test gas and
11 solution. The lids were designed to allow for the rotation of the sample and prevent the
12 application of a torsional load to the test specimen when tightening the locking ring.
13
14
15

16 The locking rings, part number 5 in Figure 1, were made of 316L grade stainless steel and
17 threaded to provide smooth travel with the threads on each end of the vessel body.
18
19

20 A notable benefit of the vessel load bearing design is that it allows data to be collected over
21 the complete 360° scan (i.e. without the presence of artefacts or shadows in images) in the X-
22 ray tomography instrument, due to the absence of load bearing side members on the vessel
23 body. The ability to lock-off the test specimen under static load is desirable in order to keep
24 the crack open during X-ray scanning. This feature was considered especially important as it
25 assists with monitoring a crack and reduces the risk of crack wedging and/or premature crack
26 closure. To achieve this requirement, the grippers shown in Figure 1 and 2 were designed and
27 built to be placed at the top and bottom of the sample after interrupting the fatigue test and
28 applying a static tensile load. Four horizontal bolts on the grippers secure the friction between
29 the sample and grippers faces. Two vertical bolts lead to a compressive load on top of the
30 compression plate. This mechanism allows keeping the tensile load in the sample applied by
31 test machine during the X-ray inspection.
32
33
34
35
36
37
38
39
40

41 The overall outer diameter of the vessel is 102mm, a value that was consistent with the
42 maximum working distance between the detector and X-ray source for the XRadia instrument
43 (i.e. no more than 110mm to get high-resolution images). The overall height of the vessel was
44 chosen to be 130mm to accommodate the ASTM standard for sample dimensions. It was
45 sufficient to allow enough space in the X-ray scanner for fittings on the top and bottom of the
46 vessel. Figure 2 shows the vessel placed inside the fatigue test machine. The gas/solution
47 inlets and outlets are also shown.
48
49
50
51
52
53
54
55
56
57
58
59
60

3. Experimental procedure

3.1. Specimen and test conditions

All experiments were carried out on specimens extracted longitudinally from parent material from X65 steel pipe with static yield strength, cyclic yield strength and ultimate tensile strength values of 516 MPa, 614 MPa and 420 MPa respectively. Two types of fatigue specimens were used in this study namely smooth (Figure 3a) and pre-pitted (Figure 3b, c). The vessel can accommodate these two sample geometries. They were designed in accordance with ASTM E466 (Figure 3a) and machined from pipes provided by the industrial sponsor. Initial trials indicated that in order to decrease the effect of beam hardening on X-ray images and optimise resolution, it was necessary to reduce the width of the pre-pitted samples from 10mm to 3mm (Figure 3b). In order to make a smooth contact between O-rings and the sample, a curved edge was designed on all specimens. Figure 3d shows the size of the fillet that was machined on the edge of all test specimens. All samples were ground to a 4000 carbon-silica paper finish prior to a final polish using a 3 μ m cloth. A corrosion pit of the desired dimensions was created in the centre of the test section of the specimen (Figure 3c) by using a VersaScan electrochemical instrument utilising the galvanostatic method and constant current of 500 μ A. The pit-to-fatigue crack transition was investigated by monitoring the pre-pitted sample during the *in-situ* corrosion fatigue test using X-ray micro-tomography.

An initial corrosion fatigue test was performed using the smooth test specimen to both check the performance of the apparatus and also obtain an estimate of the number of cycles to failure in a corrosive environment and thus plan the scanning intervals (i.e. determine the appropriate number of cycles to run before the test should be periodically interrupted and the specimen locked-off under load for X-ray tomography). The samples were tested under the constant amplitude loading condition in the high cycle fatigue regime, using a sinusoidal waveform. The applied stress ratio (R) is 0.1 for all the tests, and the maximum stress was 333 MPa for the smooth samples with cross-section of 3x10 mm² (Figure 3a), and 413 MPa for the pre-pitted sample that had cross-section of 3x3 mm² (Figure 3b).

A frequency of 0.3Hz was applied to allow the corrosive environment to interact with the sample. Testing was conducted at ambient pressure and temperature. The test environment comprised 3.5% w/v NaCl solution saturated with a gas mixture containing 12.5% H₂S in CO₂ balance.

3.2. Test protocol

The corrosion fatigue tests were performed in the Gooch laboratory at The Welding Institute (TWI Ltd.) in Cambridge, which has fixed H₂S monitoring and suitable extraction and safety procedures in place. A full risk assessment was carried out with relevant staff. Prior to starting the test, 3.5% NaCl solution was deaerated by purging with high-purity nitrogen for 24hrs in a sealed High Density Polyethylene (HDPE) barrel. Previous work at TWI has shown that this process reduces the measured dissolved oxygen content to below 10ppb. Once the apparatus and sample were assembled and placed in the fatigue machine, a leak test was carried out by pressurising the test cell with nitrogen to 0.5 barg to ensure that the seals did not leak. Following confirmation of seal integrity, the test cell was de-aerated using a fast purge of nitrogen for 1hr, then charged with 3.5% NaCl solution, and then purged once again with nitrogen for approximately one hour. Upon completion of this process, the test solution in the cell was saturated with sour test gas (i.e. containing 12.5% H₂S) using a fast purge for 1 hr. Finally, fatigue load was applied to the sample with the frequency of 0.3Hz and stress ratio of 0.1. The vessel contains about 380 cm³ of solution. Figure 4 shows the experimental setup.

To investigate the pit-to-crack transition and its evolution, the fatigue test of a pre-pitted sample was interrupted at 20,000 and 40,000 cycles, the cell contents drained and the cell filled with nitrogen to minimise the risk of air ingress in the test cell and oxidation of the specimen including crack surfaces. The presence of residual moisture retained in the cell following draining, approximately 50ml of 3.5%NaCl solution saturated with nitrogen, was anticipated to ensure that specimen and crack surfaces remained wet during X-ray scans, due to the vapour pressure of water above the salt solution (Raoult's Law) that would lead to relative humidity (%RH) values of around 80% at laboratory temperature. A tensile load equivalent to half the value of the load range was applied to the test specimen and held by tightening the grippers on the top and bottom of the specimen. Once secured, the cell was released from the fatigue test machine and put on the bespoke base and placed in the X-ray micro-tomography instrument (Figure 5). The stress applied during scanning (186 MPa) was well below the maximum cyclic stress (413 MPa) and the yield strength of the material (516 MPa), but still sufficient to hold the crack open in order to assist with imaging the crack. After each X-ray scan, taking about 13hrs, the fatigue test was resumed without any delay. The aforementioned sequence was repeated until the sample failed. No leaks of toxic H₂S (through personal or fixed laboratory sensors and alarms) have been recorded during any

1
2
3 tests. Due to the formation of electrically conducting corrosion product (i.e. iron sulphide),
4 the use of DCPD (Direct current potential drop)/ACPD (Alternating current potential drop)
5 for monitoring of crack initiation could not be considered in this study.
6
7

8 3.3. X-ray micro-computed tomography 9

10 X-ray micro-computed tomography was performed using an X-Radia 520 VersaScan
11 instrument at the National Structural Integrity Research Centre (NSIRC), Cambridge, UK. A
12 total of 1601 images were captured on a voxel size of $3.75 \times 3.75 \times 3.75 \mu\text{m}^3$ using a 150kV
13 accelerating voltage and exposure time of 27s as the entire rig was rotated through 360° . This
14 led to a scan time of approximately 13hrs. The Scout and Scan software was used to
15 reconstruct the data obtained from the laboratory X-ray source. The corrosion pit was further
16 analysed by commercially available image processing software, Avizo 9.4.
17
18
19
20
21
22

23 4. Results and discussions 24

25 The smooth sample failed at 123,880 cycles. In order to monitor the fatigue crack initiation
26 and evolution, a corrosion fatigue test using a pre-pitted sample was interrupted at 20,000
27 cycles and 40,000 cycles. A fatigue crack was observed at the second X-ray inspection. The
28 processed X-ray images taken after 40,000 cycles are shown in Figure 6. It reveals that a
29 crack initiated at the bottom of the pit with a length of $241 \mu\text{m}$ (Figure 6b). Figure 6c also
30 shows the top view of this crack that initiated from the wall. This crack subsequently
31 propagated and led to the failure of the sample at 43,000 cycles (Figure 7). In this sample, the
32 crack propagation time was very small because of the thin thickness of the sample. The crack
33 initiation site and propagation path are shown in SEM images in Figure 8. These images
34 show a single initiation point from the bottom of the pit, thus confirming our observation of
35 crack initiation site in X-ray images. Figure 9 show further cracks at the bottom of the pit that
36 did not propagate through the sample thickness. Prior to taking the SEM images, the sample
37 was cleaned in an ultrasound bath of water and Pyrene to remove all the corrosion products
38 from the surface of sample.
39
40
41
42
43
44
45
46
47

48 A key advantage of this *in-situ* corrosion fatigue procedure is that it enables the researcher to
49 monitor a crack initiated not only from the surface but also from the walls and base of the pit,
50 without the need to take the sample out of the cell and making that in contact with air. Also,
51 the detailed evolution of fatigue crack can be monitored by interrupting the test more times
52 (for example every 1000cycles) after detecting the initial crack. The outlined test protocol has
53
54
55
56
57

1
2
3 the potential to provide a thorough understanding of the pit-to-fatigue crack transition
4 mechanism by using a 3D observation at the microscale (3.75 μm) and will help to develop
5 the subject knowledge in various industries.
6
7

8 An obvious limitation of this lab-based methodology is the restricted sample size since it was
9 observed that any sample with the cross-section of more than $3 \times 3 \text{ mm}^2$ led to the increase in
10 the beam hardening effect of X-ray scanner and a decrease in the resolution of the image.
11
12

13 **5. Conclusions**

14
15 A new corrosion fatigue test methodology that allows X-ray micro-CT to be performed *in-*
16 *situ* is described. A prototype environmental cell was developed to allow *in-situ* corrosion
17 fatigue testing of axially loaded specimens in sour corrosive environments. The cell design
18 facilitates periodic X-ray micro-CT, without the need to remove the specimen from the test
19 cell. As the design allows the specimen to be scanned under load without removal from the
20 test cell, issues relating to crack closure or degradation in the air are avoided. The safe and
21 reproducible performance of the apparatus and test methodology for the study of the
22 corrosion pit-to-crack transition in X-65 steel in sour saline solutions has been demonstrated.
23
24
25
26
27
28

29 **Acknowledgment**

30
31 This publication was made possible by the sponsorship and support of BP, TWI and Coventry
32 University. The work was enabled through, and undertaken at, the National Structural
33 Integrity Research Centre (NSIRC), a postgraduate engineering facility for industry-led
34 research into structural integrity established and managed by TWI through a network of both
35 national and international Universities. The first author would like to acknowledge TWI
36 technician Jack Smith for his assistance in running corrosion fatigue tests.
37
38
39
40
41

42 **References**

- 43
44
45 1. Kristoffersen M, Børvik T, Langseth M, Hopperstad OS. Dynamic versus quasi-static
46 loading of X65 offshore steel pipes. The European Physical Journal Special Topics.
47 Springer; 2016;225(2):325–34.
48
49 2. Mohammed S, Hua Y, Barker R, Neville A. Investigating pitting in X65 carbon steel
50 using potentiostatic polarisation. Applied Surface Science. Elsevier; 2017;423:25–32.
51
52 3. Ossai CI, Boswell B, Davies IJ. Pipeline failures in corrosive environments-A
53 conceptual analysis of trends and effects. Engineering Failure Analysis. Elsevier;
54 2015;53:36–58.
55
56
57
58
59
60

- 1
 - 2
 - 3
 - 4
 - 5
 - 6
 - 7
 - 8
 - 9
 - 10
 - 11
 - 12
 - 13
 - 14
 - 15
 - 16
 - 17
 - 18
 - 19
 - 20
 - 21
 - 22
 - 23
 - 24
 - 25
 - 26
 - 27
 - 28
 - 29
 - 30
 - 31
 - 32
 - 33
 - 34
 - 35
 - 36
 - 37
 - 38
 - 39
 - 40
 - 41
 - 42
 - 43
 - 44
 - 45
 - 46
 - 47
 - 48
 - 49
 - 50
 - 51
 - 52
 - 53
 - 54
 - 55
 - 56
 - 57
 - 58
 - 59
 - 60
4. Fatoba O, Akid R. Low cycle fatigue behaviour of API 5L X65 pipeline steel at room temperature. *Procedia Engineering*. Elsevier; 2014;74:279–86.
 5. Larrosa N, Akid R, Ainsworth R. Corrosion-fatigue: a review of damage tolerance models. *International Materials Reviews*. Taylor & Francis; 2017;1–26.
 6. Turnbull A, Zhou S. Pit to crack transition in stress corrosion cracking of a steam turbine disc steel. *Corrosion science*. Elsevier; 2004;46(5):1239–64.
 7. Xu S, Wang Y. Estimating the effects of corrosion pits on the fatigue life of steel plate based on the 3D profile. *International Journal of Fatigue*. Elsevier; 2015;72:27–41.
 8. Van der Walde K, Hillberry B. Initiation and shape development of corrosion-nucleated fatigue cracking. *International Journal of Fatigue*. Elsevier; 2007;29(7):1269–81.
 9. Jones K, Hoepfner DW. Prior corrosion and fatigue of 2024-T3 aluminum alloy. *Corrosion Science*. Elsevier; 2006;48(10):3109–22.
 10. Patterson BM, Cordes NL, Henderson K, Williams JJ, Stannard T, Singh SS, et al. In situ X-ray synchrotron tomographic imaging during the compression of hyper-elastic polymeric materials. *Journal of materials science*. Springer; 2016;51(1):171–87.
 11. Cordes NL, Henderson K, Stannard T, Williams JJ, Xiao X, Robinson MW, et al. Synchrotron-based X-ray computed tomography during compression loading of cellular materials. *Microscopy Today*. Cambridge University Press; 2015;23(3):12–9.
 12. Williams JJ, Yazzie KE, Phillips NC, Chawla N, Xiao X, De Carlo F, et al. On the correlation between fatigue striation spacing and crack growth rate: a three-dimensional (3-D) X-ray synchrotron tomography study. *Metallurgical and Materials Transactions A*. Springer; 2011;42(13):3845–8.
 13. Khor K, Buffière J-Y, Ludwig W, Toda H, Ubhi H, Gregson P, et al. In situ high resolution synchrotron x-ray tomography of fatigue crack closure micromechanisms. *Journal of Physics: Condensed Matter*. IOP Publishing; 2004;16(33):S3511.
 14. Singh SS, Williams JJ, Hruby P, Xiao X, De Carlo F, Chawla N. In situ experimental techniques to study the mechanical behavior of materials using X-ray synchrotron tomography. *Integrating Materials and Manufacturing Innovation*. Springer; 2014;3(1):9.
 15. Horner D, Connolly B, Zhou S, Crocker L, Turnbull A. Novel images of the evolution of stress corrosion cracks from corrosion pits. *Corrosion Science*. Elsevier; 2011;53(11):3466–85.
 16. Buffiere J-Y. Fatigue Crack Initiation And Propagation From Defects In Metals: Is 3D Characterization Important? *Procedia Structural Integrity*. Elsevier; 2017;7:27–32.
 17. Srivatsan S, Sudarshan T. Mechanisms of fatigue crack initiation in metals: role of aqueous environments. *Journal of materials science*. Springer; 1988;23(5):1521–33.

18. Wang Y, Akid R. Role of nonmetallic inclusions in fatigue, pitting, and corrosion fatigue. *Corrosion*. 1996;52(2):92–102.
19. Akid R, Dmytrakh I. Influence of surface deformation and electrochemical variables on corrosion and corrosion fatigue crack development. *Fatigue & fracture of engineering materials & structures*. Blackwell; 1998;21(7):903–11.
20. Arriscorreta CA. Statistical Modeling for the Corrosion Fatigue of Aluminum Alloys 7075-T6 and 2024-T3. 2012.
21. Baragetti S. Notch corrosion fatigue behavior of Ti-6Al-4V. *Materials*. Multidisciplinary Digital Publishing Institute; 2014;7(6):4349–66.
22. Li S-X, Akid R. Corrosion fatigue life prediction of a steel shaft material in seawater. *Engineering Failure Analysis*. Elsevier; 2013;34:324–34.
23. Singh SS, Williams JJ, Stannard TJ, Xiao X, De Carlo F, Chawla N. Measurement of localized corrosion rates at inclusion particles in AA7075 by in situ three dimensional (3D) X-ray synchrotron tomography. *Corrosion Science*. Elsevier; 2016;104:330–5.
24. Chapman T, Kareh K, Knop M, Connolley T, Lee P, Azeem M, et al. Characterisation of short fatigue cracks in titanium alloy IMI 834 using X-ray microtomography. *Acta Materialia*. Elsevier; 2015;99:49–62.
25. Nadimi S, Kong D, Fonseca J. From imaging to prediction of carbonate sand behaviour. 2017;

Figures:

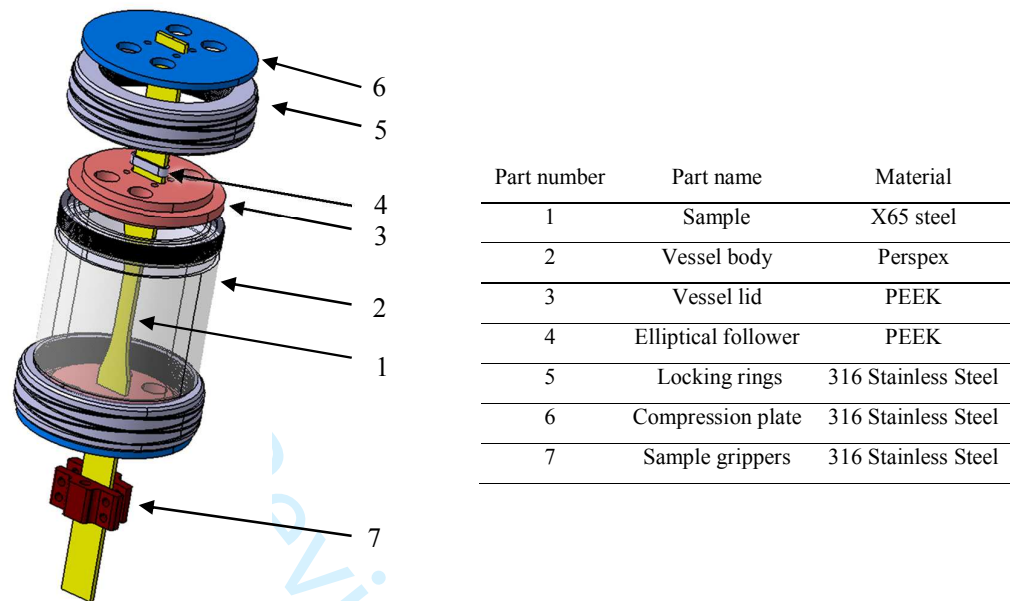


Figure1. An exploded isometric view of the *in-situ* corrosion-fatigue testing apparatus.

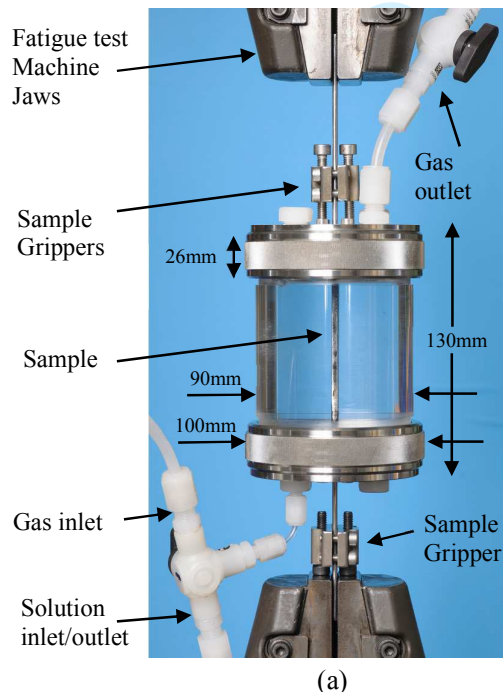


Figure 2. The corrosion fatigue test apparatus mounted in fatigue test machine showing the inlets and outlets of gas and solution and key dimensions.

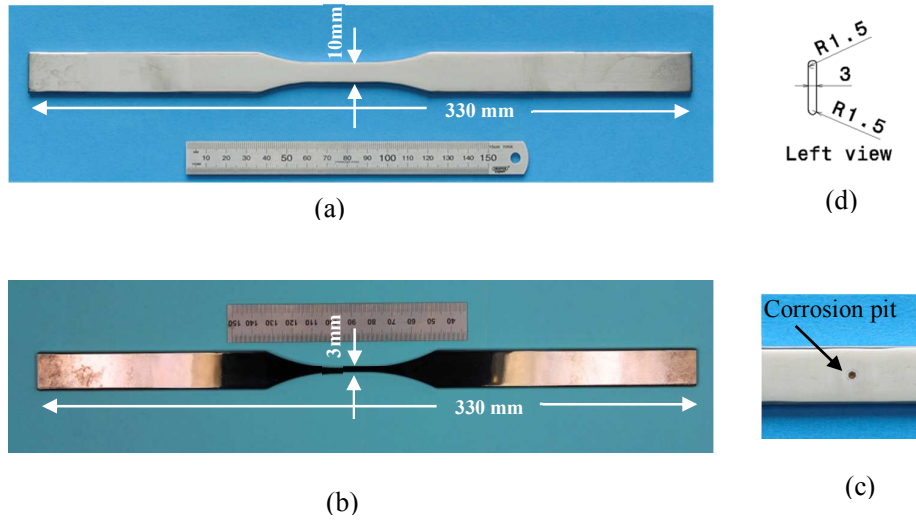


Figure 3. (a) Smooth fatigue test sample, (b) Pre-pitted fatigue test sample, (c) Close view of the pre-pitted sample, (d) Left view of the sample.

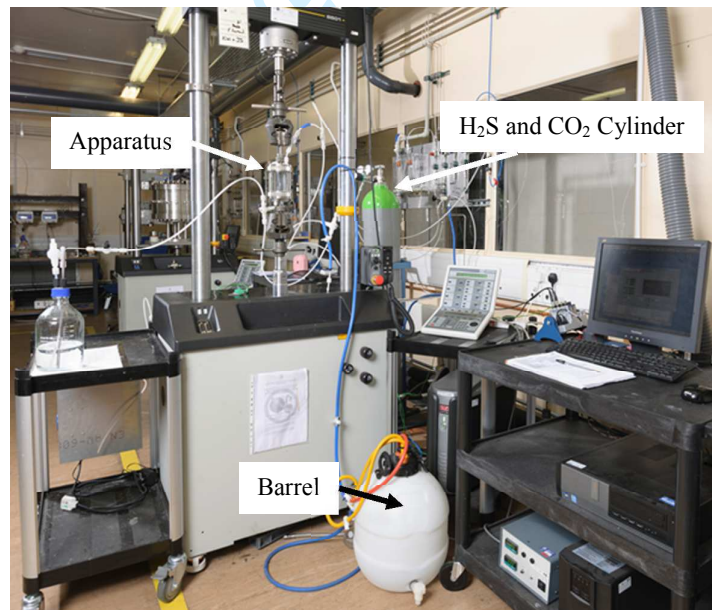


Figure 4. Experimental set up of corrosion-fatigue test.

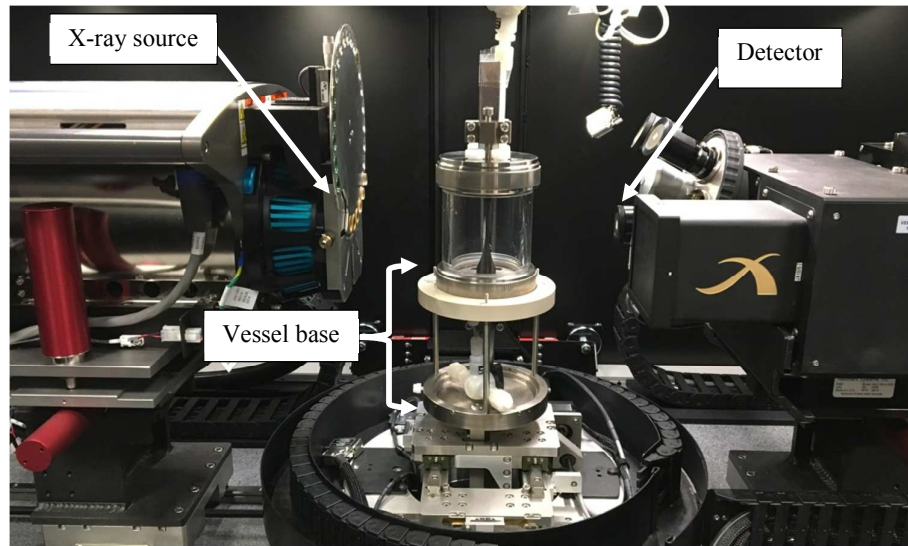


Figure 5. Test vessel inside X-ray scanner.

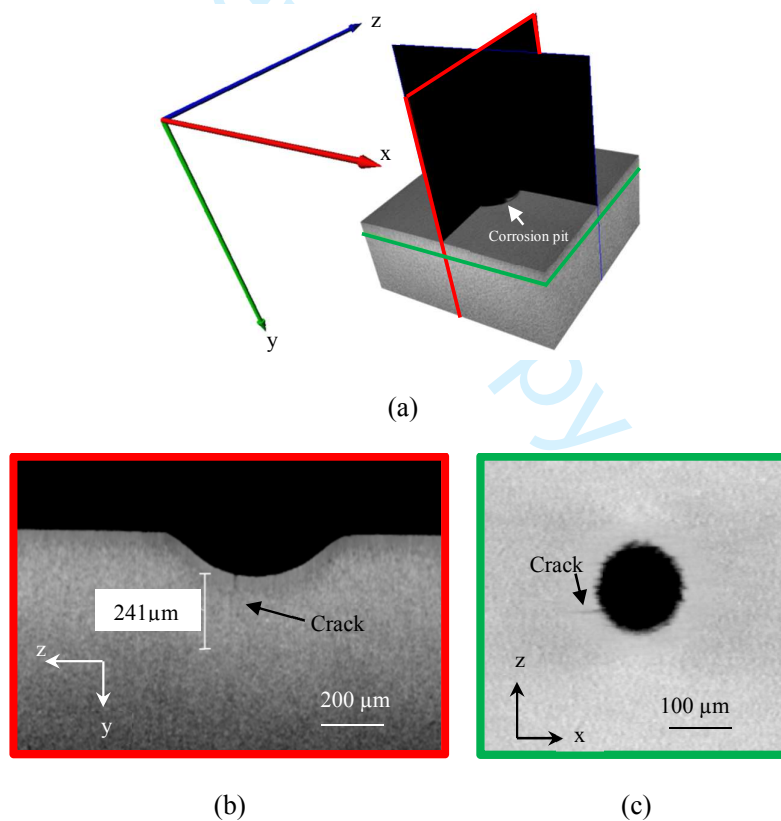


Figure 6. (a) 3D view of X-ray tomography processed images of corrosion pit after 40,000 load cycles with z-axis being the loading direction. (b), (c) y-z slice and x-z slice through the specimen showing an initiated crack from pit base.

1
2
3
4
5
6
7
8
9
10
11
12
13
14
15
16
17
18
19
20
21
22
23
24
25
26
27
28
29
30
31
32
33
34
35
36
37
38
39
40
41
42
43
44
45
46
47
48
49
50
51
52
53
54
55
56
57
58
59
60

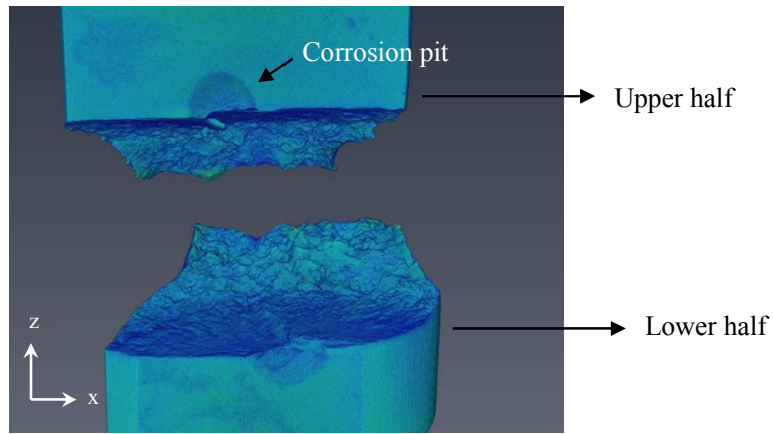


Figure7. Top view of the processed X-ray images of a failed sample.

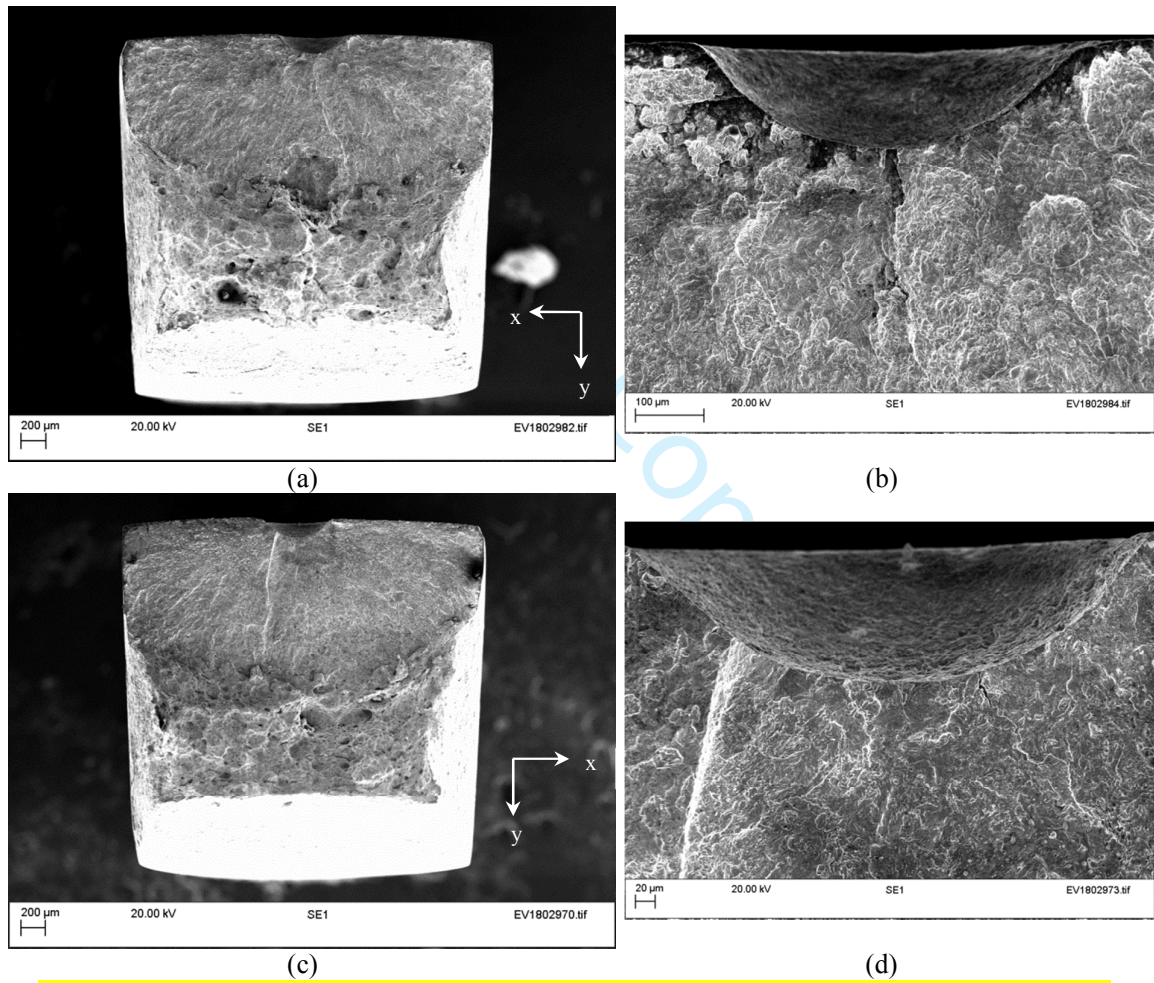


Figure8. SEM images: (a), (b) lower half, (c), (d) upper half of the failed sample (refer to Figure 7 for the upper and lower half definition).

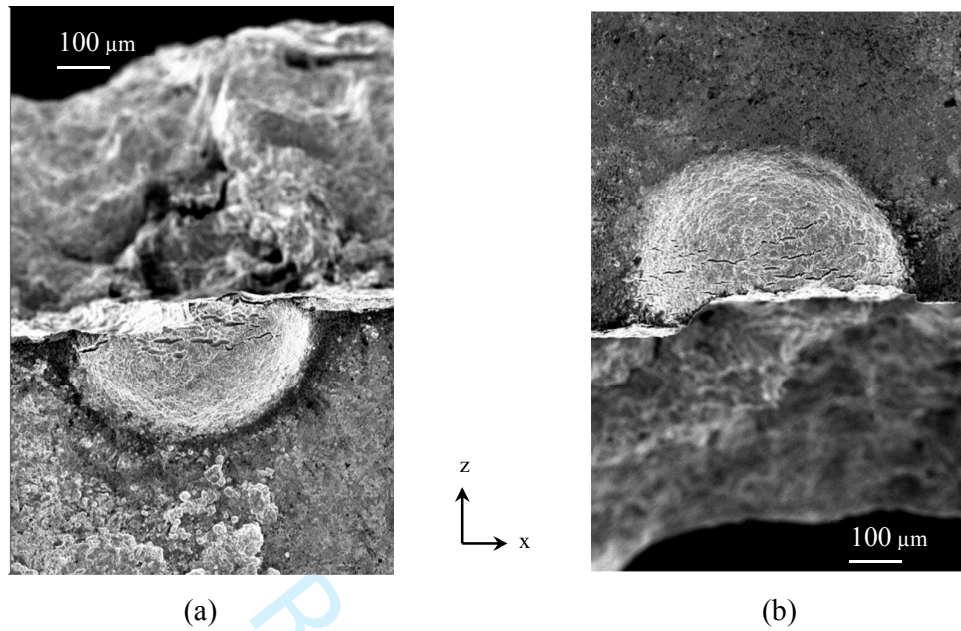


Figure 9. SEM images (a) lower half (b) upper half of the failed sample.